Journal of Biomolecular NMR, **11:** 337–354, 1998.
KLUWER/ESCOM

Solution structure of the recombinant human oncoprotein p13^{MTCP1}

Yin-Shan Yang[a], Laurent Guignard[a], André Padilla[a], François Hoh[a], Marie-Paule Strub[a], Marc-Henri Stern[b], Jean-Marc Lhoste[a] & Christian Roumestand[a,*]
[a]*Centre de Biochimie Structurale, CNRS-UMR 9955, INSERM-U414, Université de Montpellier I, Faculté de Pharmacie, 15 Avenue Charles Flahault, F-34060 Montpellier Cedex 1, France;* [b]*Unité INSERM U462 , Hôpital Saint-Louis, F-75475 Paris, France*

Received 31 July 1997; Accepted 17 October 1997

Key words: leukemia, oncogenic protein, protein structure, translocations

Abstract

The human oncoprotein p13^{MTCP1} is coded by the *MTCP1* gene, a gene involved in chromosomal translocations associated with T-cell prolymphocytic leukemia, a rare form of human leukemia with a mature T-cell phenotype. The primary sequence of p13^{MTCP1} is highly and only homologous to that of p14^{TCL1}, a product coded by the gene *TCL1* which is also involved in T-cell prolymphocytic leukemia. These two proteins probably represent the first members of a new family of oncogenic proteins. We present the three-dimensional solution structure of the recombinant p13^{MTCP1} determined by homonuclear proton two-dimensional NMR methods at 600 MHz. After proton resonance assignments, a total of 1253 distance restraints and 64 dihedral restraints were collected. The solution structure of p13^{MTCP1} is presented as a set of 20 DYANA structures. The rmsd values with respect to the mean structure for the backbone and all heavy atoms for the conformer family are 1.07 ± 0.19 and 1.71 ± 0.17 Å, when the structured core of the protein (residues 11–103) is considered. The solution structure of p13^{MTCP1} consists of an orthogonal β-barrel, composed of eight antiparallel β-strands which present an original arrangement. The two β-pleated loops which emerge from this barrel might constitute the interaction surface with a potential molecular partner.

Abbreviations: t(X;14)(q28;q11), indicates a translocation between the q28 band of chromosome X and the q11 band of chromosome 14; inv(14;14)(q11;q32), indicates an inversion between the q11 and q32 bands of chromosome 14; V(D)J, variability (diversity) joining; 2D, two-dimensional; NOE, nuclear Overhauser enhancement; NOESY, nuclear Overhauser enhancement spectroscopy; DQF-COSY, double-quantum-filtered scalar-correlated spectroscopy; z-TOCSY, z-filtered total correlation spectroscopy; CSI, chemical shift index; rmsd, root mean square deviation; DTT, 1,4-dithiothreitol; EDTA, ethylenediamine tetracetic acid; IPTG, isopropyl-thio-β-D-galactopyranoside; PMSF, phenylmethylsulfonyl fluoride; (^{2}H)TSP, 3-methylsilyl-[2,2,3,3-$^2H_4$]propionate; PEI, polyethylenimine.

Introduction

Non-random chromosomal translocations and inversions are common in human hematopoietic malignancies (Haluska et al., 1987). In B- and T-cell neoplasms, such chromosomal rearrangements often involve the loci for immunoglobulin and TCR genes, respectively, and occur during their recombination processes (Croce, 1987). These rearrangements juxtapose cellular proto-oncogenes to the enhancers of the immunoglobulin and TCR loci leading to oncogene deregulation. The characterization of numerous translocations or inversions found in immature (acute) T-cell leukemias has led to the discovery of several genes which appear to be important in the malignant transformation process (for a review, see

* To whom correspondence should be addressed.

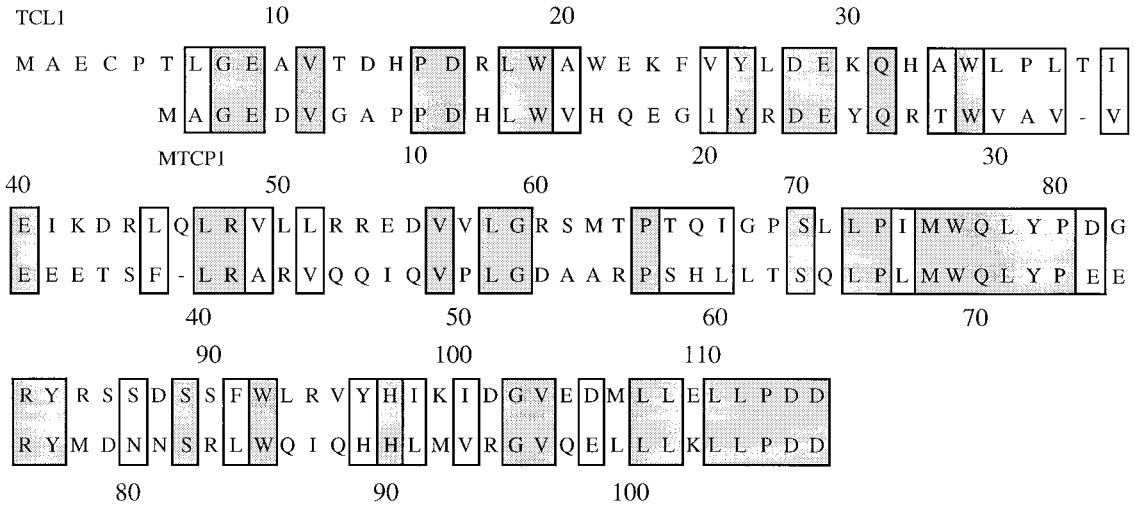

Figure 1. Homology between p13^{MTCP1} and p14^{TCL1}. The upper line shows the amino sequence of p14^{TCL1} and the lower line shows the amino sequence of p13^{MTCP1}. Dark shaded rectangles indicate identical amino acids and light shaded rectangles indicate amino acids with similar properties (hydrophobic, polar, negatively and positively charged). The two proteins have 40% identity and 59% similarity.

Rabbitts (1994)). In contrast, little is known about the genetic aberrations associated with the heterogeneous group of uncommon T-cell leukemias having a mature phenotype. Nevertheless, the translocation t(14;14)(q11;q32), or inversion inv(14)(q11;q32), and the translocation t(X;14)(q28;q11) are recurrently associated with these rare subsets of mature T-cell proliferations (Dallapiccola et al., 1984; Witzig et al., 1986; Davey et al., 1988; Russo et al., 1989; Goyns et al., 1993; Stern et al., 1993; Sherrington et al., 1994; Madani et al., 1996). These translocations, which occur during V(D)J recombination of TCR genes, are also observed in ataxia telangiectasia patients. In these patients, non-malignant clonal proliferations of T-lymphocytes bearing these translocations can be observed years before the emergence of leukemia, indicating that these chromosomal aberrations are one of the early events of the malignant transformation (for a review, see Taylor et al. (1996)). The characterization of these translocations (or inversion) has led to the discovery of two genes which appear to be important in the oncogenesis: *TCL1* (Virgilio et al., 1993; Fu et al., 1994), associated with t(14;14)(q11;q32) or inv(14)(q11;q32), and *MTCP1* (also called *c6.1B*) (Fisch et al., 1993; Stern et al., 1993), associated with t(X;14)(q28;q11). The potentially oncogenic proteins encoded by these two genes have been recently identified. *TCL1* codes for a 114 amino acid protein (14 kDa) p14^{TCL1} (Fu et al., 1994). More surprisingly, the two *MTCP1* major splicing forms, A and B, code for two entirely different proteins, a phenomenon seldom observed in mammals. Type A transcripts code for a small 8 kDa (68-residue) protein p8^{MTCP1} (Soulier et al., 1994) localized in mitochondria (Madani et al., 1995) whose 3D structure has been recently elucidated (Barthe et al., 1997). This protein is overexpressed in proliferating T-cells, but is also expressed at low levels in most human tissues (Soulier et al., 1994; Madani et al., 1996). Thus, even though p8^{MTCP1} may participate in oncogenesis, it is more likely to be associated with a function common to many cell types. The longer transcript, B1, codes for a 107-residue (13 kDa) protein known as p13^{MTCP1} (Madani et al., 1996). This protein shows high sequence similarity (40% identity) with p14^{TCL1} (Fu et al., 1994) (Figure 1). Transfection experiments have recently shown that the overexpression of p13^{MTCP1} led to malignant T-cell proliferations in mice (M.H. Stern, personal communication). Since p13^{MTCP1} and p14^{TCL1} do not share homology with other known sequences, they may constitute the first discovered members of a new family of oncogenic proteins. We present here the first report on the structure determination of a recombinant human p13^{MTCP1} by 2D homonuclear NMR.

Materials and Methods

Sample preparation

The cDNA encoding p13^{MTCP1}was subcloned into the BamH1 site of the pGEX2T vector (Pharmacia) leading to an in frame fusion with the GST gene (Madani et al., 1996). *E. coli* (BL21 cells) transformed with the recombinant plasmid were used to inoculate 400 ml of medium (trypton 20 g/l, yeast extract 10 g/l, sodium citrate 5 g/l, KH_2PO_4 5 g/l adjusted to pH 7.0) containing 100 μg/ml ampicillin. After overnight growth at 37 °C, the culture was used to inoculate 4 l of the same medium supplemented with ampicillin (100 μg/ml), $MgSO_4$ (10 mM), glucose (5 g/l), biotin (1 mg/l), thiamine (10 mg/l) and nicotinamide (10 mg/l) and grown at 37 °C for 3 h. Expression was induced for 4 h by the addition of 0.5 mM IPTG. The cells (25 g) were harvested by centrifugation for 20 min at 8000 rpm, thawed and resuspended in 100 ml of ice-cold 50 mM Tris-HCl, pH 7.5, 100 mM NaCl, 5 mM EDTA, 1 mM DTT, 5 mM benzamidine, 0.1 g/l PMSF and 0.5 mg/ml of lysozyme. The suspension was stirred on ice for 30 min and then probe sonicated for 4 min with 0.2 s bursts at 160 W. The particulate material was removed by centrifugation at 50 000 × g for 2 h and at 4 °C. PEI was added to the supernatant to a final concentration of 0.3% and the solution was stirred on ice for an additional 10 min. The precipitate was removed by centrifugation at 50 000 × g for 30 min and the supernatant was applied onto a glutathione-sepharose-6B (Pharmacia) column (2.5 cm × 2 cm) equilibrated with 50 mM Tris-HCl, pH 7.5, and 20 mM NaCl. GST cleavage was carried out on the column in 40 ml of buffer containing 20 μl of human thrombin (100 U/ml), at room temperature, overnight with gentle shaking. p13^{MTCP1} was eluted in 10 ml fractions. The protein-containing fractions were identified by 12.5% SDS-PAGE and pooled. p13^{MTCP1} was loaded onto a Q-sepharose FF (Pharmacia) column (1.6 cm × 10 cm) equilibrated in 50 mM Tris-HCl pH 7.5 and 20 mM NaCl. The column was eluted with a 250 ml linear gradient of 0.02–2 M NaCl in the above buffer and 1 ml fractions were collected at a flow rate of 1 ml/min. The fractions containing the protein, as shown by SDS-PAGE, were pooled and concentrated using an Amicon® stirred cell with a Diaflo® YM3 ultrafiltration membrane. p13^{MTCP1} was further purified by gel filtration on a Sephadex HR 100 (Pharmacia) column (1.6 cm × 100 cm) equilibrated with 50 mM sodium phosphate buffer, pH 6.5. Fractions (1 ml) were collected at a flow rate of 0.3 ml/min. The protein eluted as a single peak and the corresponding fractions were pooled and concentrated.

NMR measurements

All NMR experiments, i.e. DQF-COSY (Rance et al., 1983), z-TOCSY (Braunschweiler and Ernst, 1983; Davis and Bax, 1985; Rance, 1987), and NOESY (Jeener et al., 1979; Kumar et al., 1980), were carried out at 600 MHz (Bruker AMX600) and, generally, at 35 °C on 2 mM protein samples at pH (pD) 6.5. Deuterated reagents were purchased from EURISOTOP.

NOESY experiments were recorded with mixing times of 100 ms. z-TOCSY experiments were carried out using the TOWNY isotropic transfer sequence (Kadkhodaei et al., 1993) and mixing times ranging from 30 to 60 ms. In all 2D experiments, quadrature detection in the indirectly observed dimension was obtained with States-TPPI (Marion et al., 1989). Solvent suppression in z-TOCSY and NOESY experiments was carried out using the WATERGATE method (Piotto et al., 1992) in association with water-flip-back pulses (Lippens et al., 1995; Dalhuin et al., 1996). In DQF-COSY experiments, water suppression was obtained with a low-power irradiation of the solvent signal during the relaxation delay. The spectral width used in both dimensions was 10 000 Hz; 4K complex data points in t_2 and 512 experiments in t_1 were usually acquired, except for DQF-COSY where 800 experiments were acquired in t_1. Typically, 128 scans (NOESY, DQF-COSY) or 96 scans (z-TOCSY) were acquired per increment.

The data sets were processed using GIFA (Pons et al., 1996). NH-C^{α}H and C^{α}H-C^{β}H coupling constants were measured in the DQF-COSY spectra (2 Hz of digital resolution). In order to compensate for the overestimation of the $^3J_{NH-H\alpha}$ due to the broad linewidth of the antiphase multiplets, we used the method previously described by Ludvigsen et al. (1991), using a macro implemented in GIFA. Spin systems determination and sequential assignment of the ^{1}H resonances were computer-assisted using the in-house CINDY software (A. Padilla, to be published), operating on a Silicon Graphics O_2 workstation.

Molecular modelling calculations

Calculations were carried out on Hewlett-Packard HP735 or SGI R5000 and R10000 workstations. The volumes of cross peaks were integrated in the 100 ms NOESY spectra and were classified as strong, medium and weak, and converted to the corresponding upper-

limit distance constraints of 2.8, 3.6, and 4.4 Å, respectively. Very strong cross peaks involving residues in extended strands were converted into an upper limit of 2.4 Å. A total of 39 ϕ dihedral angles were restrained to $-120 \pm 50°$, as deduced from the empirically calibrated Karplus relation (Karplus, 1963; Pardi et al., 1984) applied to the coupling constant $^3J_{NH-H\alpha}$ values ($\geq$8 Hz) measured in the DQF-COSY. Twenty-five χ_1 angles were obtained from the analysis of the $^3J_{H\alpha-H\beta}$ coupling constants and intraresidue NOEs (Hyberts et al., 1987). The limits of the intervals were set to $\pm 30°$. When no stereospecific assignment was possible, pseudoatoms were defined and corrections added as described by Wüthrich et al. (1983). No additional restraints were used for hydrogen bonds.

3D structures were deduced from the experimental distance and angle restraints using the torsion angle dynamic algorithm recently implemented in the DYANA program (v. 1.3; Güntert et al., 1997). Each run started from 300 randomized conformers. The analysis of the first generated structures allowed us to resolve ambiguities in the assignment of NOE cross peaks arising from chemical shift degeneracy and thus the derivation of additional interproton restraints. This procedure was iterated several times by calculating a new set of structures with an improved list of restraints at each step. From the 300 structures generated with the final list of restraints, a set of 20 structures, with the lowest target functions, was selected for further analysis. The structures were displayed and analyzed on a Silicon Graphics O_2 station using the INSIGHT program (v. 95, Biosym Technologies, San Diego, CA).

Results

Resonance assignments

NMR experiments were performed on a sample obtained following a protocol close to that previously published by Madani et al. (1996) (see the Materials and Methods section): 10 residues (two residues at the N-terminus and eight at the C-terminus) were added to the sequence of p13^{MTCP1} for subcloning facilities and in order to prevent enzymatic degradation (Madani et al., 1996), leading to a 117 amino acid protein. The assignment of proton resonances by classical ^{1}H 2D NMR techniques therefore appeared rather challenging. But spectral overlap represented less of a problem due to the extremely good resonance dispersion in the protein ^{1}H spectra: the amide proton resonances spread over more than 4 ppm, and methyl group resonances were observed up to -1.2 ppm. This latter property resulted in a surprisingly well-resolved methyl spectral region, unexpected given the number of leucine (14), valine (9) and isoleucine (4) residues, which appear along hydrophobic stretches throughout the protein sequence (see, for example, the peptidic segment 99–104 in Figure 2).

Analysis of DQF-COSY and TOCSY spectra recorded in H_2O, generally at 35 °C, provided the starting points for the assignment of p13^{MTCP1} proton resonances. Whereas a poor transfer of magnetization during the TOCSY transfer stages was observed for most spin systems, leading to vanishingly weak cross peaks when long mixing periods ($\geq$60 ms) were used, the spin systems of residues located in the flexible N- (Ser^0–Ala^8) and C- (Gly^{111}-Asp^{115}) termini gave sharp and intense TOCSY cross peaks, in association with strong $d_{\alpha N}(i, i+1)$ sequential NOEs. Their sequential assignment was thus relatively straightforward, using the strategy described by Wüthrich (1986). The assignment of the spin systems constitutive of the structured core of p13^{MTCP1} was more difficult, primarily due to the poor quality of the TOCSY spectra. Due to relatively short T_2 values, TOCSY mixing periods were kept short (typically $\leq$40 ms), and cross peaks from amide resonances were either weak or not observed for protons beyond $C^\beta H$ in the side chain. Thereby, most of the AMX, alanine and threonine spin systems could be identified but they often constituted ambiguous starting points for the sequential assignment. Some long-chain spin systems were nevertheless assigned, thanks to the redundancy of the information available from either the amide or the $C^\alpha H$ resonances, and aromatic spin systems were also unequivocally identified from NOESY spectra. The NOESY spectra in H_2O revealed strong $d_{\alpha N}(i, i+1)$ contacts which led to the recognition of short stretches of adjacent residues. Unequivocally identified side chains were used to position these stretches within the sequence of p13^{MTCP1}. The main-chain directed (MCD) strategy (Englander and Wand, 1987) was then used to complete our assignments. Fifty residues out of 117 have their $C^\alpha H$ proton resonance shifted downfield from the random-coil values (Figure 2) (Wishart et al., 1991): in association with the scarcity of sequential d_{NN} NOEs, the presence of intense $d_{\alpha N}$ NOEs and numerous $d_{\alpha\alpha}$ NOEs (Figure 3), and the strong values of most measured $^3J_{NH-H\alpha}$ coupling constants, this strongly indicates the predominancy of β-sheet structures. The long-range $d_{\alpha\alpha}$, $d_{\alpha N}$

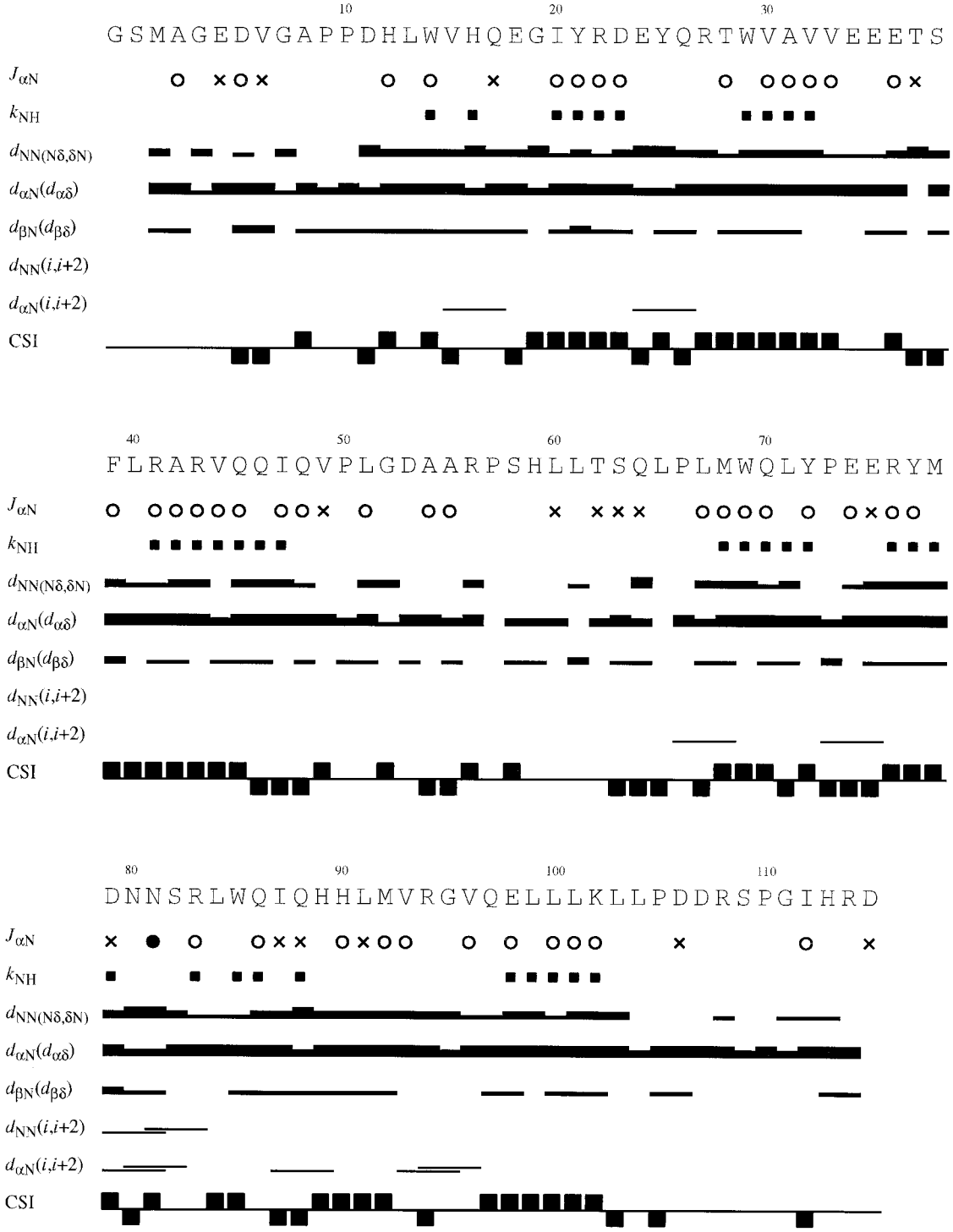

Figure 2. Summary of the sequential NOE connectivities and other NMR data for p13^{MTCP1}. NOEs are indicated by $d_{\alpha N}$, $d_{\beta N}$ and d_{NN} for the NOE contacts between $C^{\alpha}H$, $C^{\beta}H$ or NH protons of the current residue and the following residue. The thickness of the lines reflects the intensity of the NOE cross peaks (strong, medium and weak). $^{3}J_{HN-H\alpha} < 6$ Hz: filled circles; $^{3}J_{HN-H\alpha} > 8$ Hz: open circles; and $6 < ^{3}J_{HN-H\alpha} < 8$ Hz: symbol x. Slowly exchanging amide protons are indicated as filled squares. These protons were identified on NOESY or TOCSY spectra recorded at 25 °C on a sample freshly dissolved in D_2O. At the bottom, the CSI (Wishart et al., 1991) is given as positive or negative bars.

and d_{NN} NOEs were then used to extend the assignment of the previously identified peptidic segments to the whole protein. Thus, combining the results from the sequential assignment strategy and the MCD strategy allowed us to assign virtually all the proton resonances of p13^{MTCP1} (Table 1).

Secondary structure

As previously noted, a careful inspection of the NOESY spectra shows that β-sheet structures are the predominant element of secondary structure found in p13^{MTCP1}. Eight peptide segments exhibited long-range NOE contacts aligned with a perpendicular disposition with respect to the diagonal when plotted into the contact map (data not shown). This suggests the presence of an eight-stranded antiparallel β-sheet. This secondary structure element contains 33 out of the 35 slowly exchanging NH protons in the entire protein. The eight-stranded β-sheet could be divided into two similar four-stranded β-sheet motifs, connected by a long loop encompassing residues Gln^{48}–Pro^{66}. Each motif consists of a short double-stranded β-sheet (residues 11–15 (strand A), 20–23 (strand B) and residues 67–71 (strand E), 76–79 (strand F), respectively) hydrogen-bonded to a larger double-stranded β-sheet (residues 28–36 (strand C), 39–47 (strand D) and residues 84–93 (strand G), 96–103 (strand H), respectively), forming a same layer of antiparallel β-sheet (Figure 4). Each β-sheet motif is roughly similar, except for the presence of a β-bulge at positions 88–89 in the large β-sheet in the second motif (strands G and H). Regular patterns of NOE contact and hydrogen bonds were found between strands A and E and strands D and H, suggesting that these two β-sheet motifs form a continuous sheet rolled up in a β-barrel.

Calculation, description, and statistical analysis of the NMR solution structure of p13^{MTCP1}

A total of 1317 structural (distance and dihedral, Table 2) constraints were collected and taken into account for structure calculations using DYANA (Güntert et al., 1997) (see the Materials and Methods section). Of the final 300 calculated structures, 150 had a final target function smaller than 5 Å^2 and satisfy all experimental constraints with no NOE distance constraint violation exceeding 0.5 Å and no dihedral angle violation exceeding 5°. These results reflect the efficiency of the torsion angle dynamic algorithm used for DYANA calculations, both in terms of the high convergence of the calculations and the quality of the structure obtained. In the following, we restrict the discussion to a subset comprising the 20 structures with the best target value (<2.5 Å^2) and with no NOE distance violation exceeding 0.35 Å and no dihedral angle violation exceeding 3.5°, which was considered representative for the conformational space consistent with the experimental data. The survey of the structural statistics and of the residual violations of experimental constraints for these 20 conformers is shown in Table 2. Inspection of the Ramachandran plot (ProCheck; Laskowski et al., 1993) built from the energy-minimized (Pearlman et al., 1995) average structure calculated from these 20 structures shows that 74 residues (i.e. 73.3%) – out of 83 'meaningful' residues – fall in the most favored regions, 25 residues (i.e. 24.8%) are in the additional allowed regions, and only two residues (2%) fall in the generously allowed region (Ala^2 and Glu^4). These two residues are located in the disordered N-terminal end of the protein.

The main structural motif of p13^{MTCP1} consists of a β-barrel formed by an array of eight β-strands, arranged in an antiparallel manner (Figure 5). As previously suggested, the eight β-strands can be pictured as belonging to two right-handed curved four-stranded β-sheets. The first group of β-strands includes those labelled A–D in Figure 5, and the second includes those labelled E–H. Inspection of the hydrogen-bonding (Table 2) and of the ϕ and ψ angle values showed that the number of residues in the successive strands in the barrel is 5 (A), 4 (B), 9 (C), 9 (D), 8 (H), 10 (G, with a β-bulge involving residues Gln^{88}-His^{89}), 4 (F) and 5 (E). The average values of the backbone dihedral angles measured in these β-sheets are (ϕ, ψ, ω) = ($-120°$, 125°, 180°), which correspond to a moderate right twisting of the strands (Chou et al., 1990). In each motif, the two longer strands (C,D and G,H, respectively) form a larger two-stranded β-sheet. Due to the gap in the number of residues between the adjacent strands B,C and G,F, a large peptidic segment in each large β-sheet (Ala^{31}-Ser^{38} and Ile^{87}-Gly^{95} in strands C and G, respectively, including the corresponding β-hairpins) is not hydrogen-bonded to the barrel itself. With the corresponding peptidic segment in the complementary strand of the β-sheet, they form two short β-pleated loops protruding from each top of the β-barrel, in an opposite direction. Each β-sheet motif has the β-strand hydrogen-bonded in a consecutive manner following the $n, n+1$ rule – i.e. the nearest antiparallel strand is also adjacent in the amino acid sequence – and uses hairpin turns as β-strand connectors. In each β-sheet motif, the connection between the longer strands (C,D and G,H, respectively)

Table 1. Proton chemical shift assignments for p13^{MTCP1} at pH 6.5 and 35 °C

	HN	$C^{\alpha}H$	$C^{\beta}H$	$C^{\gamma}H$	Others
Gly $^{-1}$					
Ser^{0}	8.03	4.53	3.71		
Met^{1}	8.55	4.48	1.96, 2.07	2.57, 2.50	
Ala^{2}	8.35	4.30	1.34	–	
Gly^{3}	8.30	3.93, 3.88	–	–	
Glu^{4}	8.19	4.22	1.85, 1.77	2.16, 2.01	
Asp^{5}	8.26	4.54	2.64, 2.53	–	
Val^{6}	7.92	3.97	1.73	0.56, 0.44	
Gly^{7}	7.90	3.92, 3.85	–	–	
Ala^{8}	8.14	4.62	1.35	–	
Pro^{9}	–	4.15	1.38, 2.07	1.77, 1.81	H^{δ} 3.57, 3.80
Pro^{10}	–	4.47	1.80, 1.71	1.06, 1.16	H^{δ} 3.14, 3.38
Asp^{11}	10.69	4.33	2.49, 2.12	–	
His^{12}	8.18	4.99	2.42, 2.54	–	$H^{\epsilon 1}$ 8.21; $H^{\delta 2}$ 6.26
Leu^{13}	8.28	4.44	0.94, 1.59	0.70	H^{δ} −0.30, −0.57
Trp^{14}	9.48	5.42	3.35, 3.24	–	$H^{\delta 1}$ 7.14
					$H^{\epsilon 3}$ (H4) 7.58
					$H^{\zeta 3}$ (H5) 6.89
					$H^{\eta 2}$ (H6) 6.98
					$H^{\zeta 2}$ (H7) 6.90
					$H^{\epsilon 1}$ 10.17
Val^{15}	8.71	3.32	1.85	0.75, 0.38	
His^{16}	9.26	4.68	2.88, 2.79	–	$H^{\delta 2}$ 6.95; $H^{\epsilon 1}$ 7.73
Gln^{17}	7.92	4.29	1.75, 1.84	2.12	H^{ϵ} 6.77, 7.48
Glu^{18}	8.84	3.79	1.94	2.11, 2.20	
Gly^{19}	9.18	4.43, 3.73	–	–	
Ile^{20}	8.62	5.20	1.69	1.25, 1.57	$H^{\gamma 2}$ 0.96
Tyr^{21}	9.95	5.13	2.79, 2.63	–	H^{δ} 6.72; H^{ϵ} 6.23
					HO 8.87
Arg^{22}	9.26	5.93	1.92, 1.81	1.62	H^{δ} 3.04
Asp^{23}	8.11	5.63	3.60, 2.63	–	
Glu^{24}	10.96	4.10	1.83, 1.54	1.14	
Tyr^{25}	8.62	4.79	2.89, 3.46	–	H^{δ} 7.06; H^{ϵ} 6.86
Gln^{26}	8.53	3.81	2.46, 2.38	2.59	H^{ϵ} 7.49, 6.83
Arg^{27}	8.64	4.57	1.42, 1.45	–	
Thr^{28}	8.24	5.22	4.17	1.23	
Trp^{29}	9.61	5.50	2.96, 2.93	–	$H^{\delta 1}$ 6.96
					$H^{\zeta 3}$ (H5) 6.78
					$H^{\eta 2}$ (H6) 6.90
					$H^{\zeta 2}$ (H7) 7.15
					$H^{\epsilon 1}$ 11.03
Val^{30}	9.65	5.13	2.09	1.01, 1.04	
Ala^{31}	9.45	5.55	1.36	–	
Val^{32}	8.51	4.53	2.14	1.01, 0.98	
Val^{33}	8.61	4.53	2.02	1.00, 1.05	
Glu^{34}	8.89	4.57	1.87	2.01	
Glu^{35}	8.71	4.74	2.01, 1.88	2.17	
Glu^{36}	8.26	4.48	1.59	2.15, 2.00	
Thr^{37}	8.54	3.95	4.22	1.21	
Ser^{38}	8.16	4.26	3.75, 3.66	–	

Table 1. Continued

	HN	$C^{\alpha}H$	$C^{\beta}H$	$C^{\gamma}H$	Others
Phe[39]	7.56	4.79	3.09, 2.86	–	H^{δ} 7.16; H^{ϵ} 7.24
Leu[40]	8.56	4.74	1.60, 1.60	1.47	H^{δ} 0.91, 0.49
Arg[41]	8.77	5.74	1.86, 1.68	1.60	H^{δ} 2.93
Ala[42]	9.38	5.36	1.05	–	
Arg[43]	9.02	4.78	1.84	1.45, 1.25	H^{δ} 3.37, 2.98; H^{ϵ} 8.51
Val[44]	9.43	5.18	1.90	0.68, 0.17	
Gln[45]	9.29	5.61	2.07, 1.73	2.47, 2.24	H^{ϵ} 8.15, 6.50
Gln[46]	8.40	3.96	1.69, −0.10	1.00, 0.42	H^{ϵ} 8.31, 6.23
Ile[47]	7.06	4.10	1.55	1.28	$H^{\gamma 2}$ 0.91; H^{δ} 0.73
Gln[48]	8.40	4.23	1.95	2.31	H^{ϵ} 7.43, 6.74
Val[49]	7.80	4.57	2.06	0.87, 0.81	
Pro[50]	–	4.34	1.81, 2.19	1.91, 2.04	H^{δ} 3.58, 3.70
Leu[51]	8.21	4.30	1.27	1.59	H^{δ} 0.59
Gly[52]	8.48	4.11, 3.83	–	–	
Asp[53]	8.28	4.54	2.63, 2.53	–	
Ala[54]	8.16	3.90	1.26	–	
Ala[55]	8.09	4.25	1.31	–	
Arg[56]	8.16	4.51	1.59, 1.80	–	H^{δ} 3.09
Pro[57]	–	4.76	1.60, 2.20	1.92, 1.96	H^{δ} 3.58, 3.77
Ser[58]	8.34	4.24	3.87, 3.79	–	
His[59]	8.17	4.62	2.22, 3.12	–	$\eta^{\delta 2}$ 6.96; $H^{\epsilon 1}$ 7.84
Leu[60]	7.85	4.28	1.37	1.52	H^{δ} 0.74
Leu[61]	7.78	4.29	1.69, 1.69	1.59	H^{δ} 0.85, 0.60
Thr[62]	7.87	4.30	4.22	1.17	
Ser[63]	7.83	4.36	3.83, 3.92	–	
Gln[64]	8.53	4.22	1.94, 2.22	2.36, 2.36	H^{ϵ} 7.40, 6.71
Leu[65]	7.78	4.41	1.68, 1.48	1.62	H^{δ} 0.99, 0.87
Pro[66]	–	4.42	1.84, 1.61	0.62, −0.23	H^{δ} 3.14, 2.20
Leu[67]	7.76	3.97	1.33, 1.39	1.67	H^{δ} 0.78, 0.68
Met[68]	7.34	5.20	2.17, 2.00	1.85, 1.74	
Trp[69]	8.78	4.88	2.48, 2.33	–	$H^{\delta 1}$ 5.02 $H^{\epsilon 3}$ (H4) 6.25 $H^{\zeta 3}$ (H5) 4.92 $H^{\eta 2}$ (H6) 5.88 $H^{\zeta 2}$ (H7) 4.94 $H^{\epsilon 1}$ 6.02
Gln[70]	9.26	5.04	2.18, 2.06	2.24, 2.46	H^{ϵ} 7.67, 7.01
Leu[71]	9.14	3.49	1.62, 1.41	1.22	H^{δ} 0.61, 0.11
Tyr[72]	9.23	4.78	2.82, 2.75	–	H^{δ} 7.24; H^{ϵ} 6.77
Pro[73]	–	4.28	2.33	1.83, 1.73	H^{δ} 3.35, 2.84
Glu[74]	8.71	3.83	2.11	2.34	
Glu[75]	8.60	3.56	2.35, 2.14	2.08	
Arg[76]	6.79	5.28	1.51, 1.47	1.79, 1.69	H^{δ} 3.15, 2.98; H^{ϵ} 6.84
Tyr[77]	9.26	5.11	2.56, 2.26	–	H^{δ} 6.32; H^{ϵ} 6.05
HO 9.22					
Met[78]	9.62	5.47	2.72, 1.83	2.24, 1.22	H^{ϵ} 1.74
Asp[79]	9.26	5.85	3.01, 2.42	–	
Asn[80]	8.10	–	2.20, 2.79	–	H^{δ} 7.46, 7.70
Asn[81]	9.04	4.98	2.99, 2.76	–	H^{δ} 7.67, 6.86
Ser[82]	8.16	4.50	4.16, 4.09	–	

Table 1. Continued

	HN	$C^{\alpha}H$	$C^{\beta}H$	$C^{\gamma}H$	Others
Arg^{83}	8.37	4.42	1.55, 2.42	1.46, 1.64	H^{δ} 3.08, 3.27; H^{ϵ} 7.96
Leu^{84}	8.60	5.23	1.76, 1.11	1.57	H^{δ} 0.85, 0.53
Trp^{85}	9.66	5.24	2.99, 2.86	–	$H^{\delta 1}$ 7.48
					$H^{\epsilon 3}$ (H4) 7.18
					$H^{\zeta 3}$ (H5) 6.86
					$H^{\eta 2}$ (H6) 7.48
					$H^{\zeta 2}$ (H7) 7.04
					$H^{\epsilon 1}$ 12.20
Gln^{86}	9.58	4.43	2.04	2.19	H^{ϵ} 7.49, 6.76
Ile^{87}	8.69	4.06	1.83	0.44	$H^{\gamma 2}$ 0.66; H^{δ} 0.36
Gln^{88}	9.53	4.20	1.81	2.19	H^{ϵ} 7.36, 6.58
His^{89}	7.43	4.74	3.48, 3.05	–	$H^{\delta 2}$ 6.65; $H^{\epsilon 1}$ 7.79
His^{90}	8.73	5.94	3.22, 2.73	–	$H^{\delta 2}$ 6.87
Leu^{91}	8.95	4.60	1.52	1.23	H^{δ} 0.64, 0.22
Met^{92}	8.30	4.92	1.76	2.27	H^{ϵ} 1.79
Val^{93}	9.17	4.09	1.86	0.81, 0.72	
Arg^{94}	9.28	3.74	1.91, 1.79	1.55	H^{δ} 3.22
Gly^{95}	8.32	4.06, 3.49	–	–	
Val^{96}	7.71	4.25	2.01	0.77, 0.73	
Gln^{97}	8.98	4.59	2.20, 1.90	1.80	H^{ϵ} 7.44
Glu^{98}	9.53	5.58	2.21, 1.94	2.12	
Leu^{99}	9.66	5.21	1.05	1.35	H^{δ} 0.42, 0.06
Leu^{100}	8.12	5.02	0.94, 0.30	1.01	H^{δ} 0.64, 0.55
Leu^{101}	9.15	5.39	1.70, 1.14	0.95	H^{δ} 0.36, −1.20
Lys^{102}	9.33	5.03	1.71, 1.57	1.14	H^{δ} 1.32
Leu^{103}	8.23	3.33	1.41, −0.51	0.91	H^{δ} 0.51, −0.14
Leu^{104}	8.63	4.64	1.76, 1.76	1.38	H^{δ} 0.80, 0.87
Pro^{105}	–	4.27	2.25, 1.86	1.98	H^{δ} 3.86, 3.61
Asp^{106}	8.42	4.55	2.70, 2.51	–	
Asp^{107}	8.29	4.56	2.65, 2.51	–	
Arg^{108}	8.22	4.29	1.88	1.77, 1.62	H^{δ} 3.15*, 3.10*; H^{ϵ} 7.50
Ser^{109}	8.24	4.67	3.81	–	
Pro^{110}	–	4.43	2.24*	1.97*	H^{δ} 3.76*, 3.68*
Gly^{111}	8.35	3.88	–	–	
Ile^{112}	7.81	4.11	1.76	1.10, 1.32	$H^{\gamma 2}$ 0.81; H^{δ} 0.79
His^{113}	8.53	4.62	2.22, 3.13	–	$H^{\delta 2}$ 7.95; $H^{\epsilon 1}$ 7.10
Arg^{114}	8.30	4.34	1.79	1.56, 1.65	H^{δ} 3.14; H^{ϵ} 7.19*
Asp^{115}	8.01	4.34	2.66, 2.49	–	

(^{2}H)TSP was used as internal reference.
*: chemical shifts at 25 °C.

uses classical β-turns involving four residues (Glu^{36}-Thr^{37}-Ser^{38}-Phe^{39} and Val^{93}-Arg^{94}-Gly^{95}-Val^{96}, respectively) with the corresponding i, i + 3 hydrogen bonds. On the basis of the φ, ψ angle average values, the β-turn between strands G and H has been classified as a type-III' β-turn. The lack of experimental restraints precludes any classification of the β-turn between strands C and D. All the connections with at least a short β-strand involve five residues. The five-residue hairpin between strands A and B combines a canonical type-II β-turn, with the corresponding i, i + 3 hydrogen bonds, with an additional residue inserted in a bulge between the end of strand A and the first residue of the β-turn. On the three other β-hairpins, the statistical analysis of the 20 conformers does not indicate any well-defined hydrogen-bond

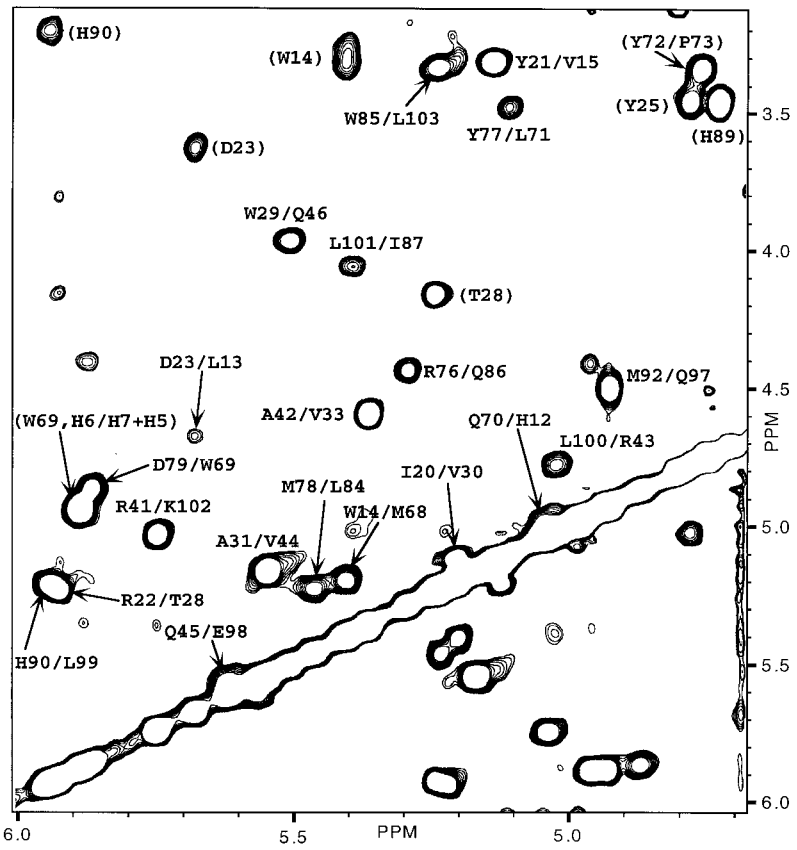

Figure 3. NOESY spectrum ($C^{\alpha}H$ proton region) of $p13^{MTCP1}$ (600 MHz, 100 ms mixing time) recorded in D_2O at pH 6.5 and 35 °C. The numerous $C^{\alpha}H$-$C^{\alpha}H$ NOEs strongly suggest the presence of antiparallel β-sheets in the secondary structure of $p13^{MTCP1}$. Cross peaks assigned in parentheses correspond to intraresidual or sequential $C^{\alpha}H$-$C^{\beta}H$ NOEs.

patterns, and these turns cannot be classified into canonical structures. Such connections involving five residues locally increase the relative angle between adjacent short strands, allowing a twisted arrangement of these strands in the β-barrel. The relative orientation of the two β-sheet motifs across the barrel is orthogonal, and their relative connection does not follow the n, n + 1 rule, since hydrogen bonds are observed between n, n + 4 β-strands (A,E and D,H). This leads to an unusual and hitherto unobserved strand arrangement in an eight-stranded barrel, a topology possible due to the long loop (residues Gln^{48} to Pro^{66}) connecting the two motifs.

Analysis of the angular order parameters (S) (Hyberts et al., 1992) (Figure 6) of the 20 selected DYANA conformers of $p13^{MTCP1}$ indicates that the two β-sheet motifs of $p13^{MTCP1}$, including β-strands and β-hairpins, are well defined in the NMR structure, with $S \geq 0.95$ for both ϕ and ψ angles (Figures 6C and D), with the sole exception of the segment Glu^{34}-Glu^{35}-Glu^{36}-Thr^{37}-Ser^{38} in strand C where lower S values are observed. This highly polar peptidic segment belongs to the β-pleated loop formed by strands C and D in the first β-sheet motif and is not hydrogen-bonded to the β-barrel itself. It is thereby solvent-exposed, as experimentally supported by the fact that the NH resonances of its constitutive residues were found to exchange with water, presumably leading to an inaccurate quantification of the NOE constraints. S parameters close to 1 are observed for χ_1 angles of most residues whose side chains face the interior of the barrel (Figure 6E), indicating that their position is well defined, despite the fact that stereospecific assignment of the H^{β} protons was not available for all of these residues. The good definition of these χ_1 angles (and also of most of the χ_2 angles: see Figure 7) is presumably a consequence of the close packing of the inward pointing side chains rather than the direct experimental data. The N- and C-termini, and to a lesser extent the long loop connecting the two β-sheet motifs, are less

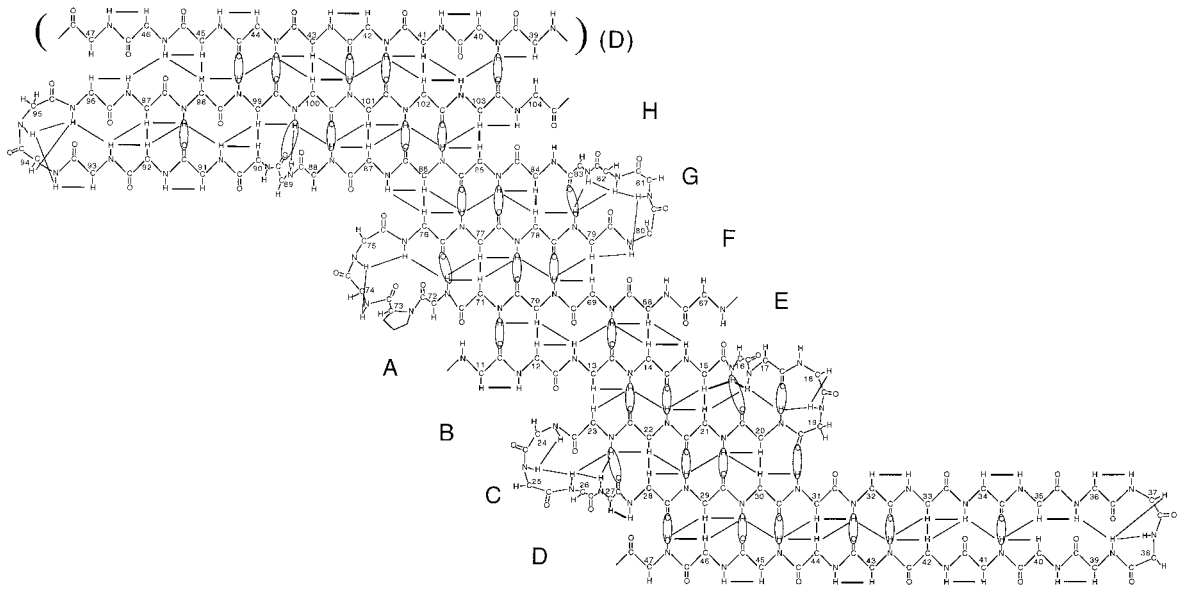

Figure 4. Identification of the antiparallel β-sheet in the secondary structure of p13^{MTCP1}. The solid lines between backbone protons indicate the observed NOEs. The ellipses between amide protons and carbonyl groups indicate the hydrogen bonds identified on the regular β-sheet structure on the basis of the exchange rate of the corresponding amide protons. Amide protons were considered as engaged in a hydrogen bond when corresponding cross peaks were still visible on TOCSY or NOESY spectra recorded at 25 °C on a freeze-dried protein sample freshly dissolved in D_2O.

well defined, presumably a consequence of increased flexibility.

Similar conclusions can be drawn from the backbone rmsd values (Figure 6B and Table 2): in conjunction with the high number of NOEs per residue (Figure 6A), the low rmsd values measured for the two β-sheets indicate that they are well defined.

Discussion

Analysis of known protein structures has shown that they are often organized into smaller units called domains, which display a limited repertoire of folding patterns. One such pattern is the β-barrel. The very high number of functionally unrelated proteins which adopt this folding pattern (Branden and Tooze, 1991) suggests that β-barrels are stable building blocks onto which different functionalities can be designed. Murzin et al. (1994a) have shown that all the general structural features of regular β-sheet barrels can be deduced from only two parameters: n, the number of strands in the β-sheet, and S, the shear number. S measures the stagger of the strands in the β-sheet, thus reflecting the tilting of the β-barrel. It is calculated as follows: starting at a given residue *i* in the first strand and moving around the barrel in a direction perpendicular to the direction of the strands, one would arrive back to the first strand at residue $i + S$, i.e. at S residues further along the strand. The β-barrel found in p13^{MTCP1} is made up of eight strands, and has a shear number of 10. A positive value of S corresponds to a right-tilted barrel, the energetically favored structural pattern of antiparallel β-barrels in protein (Chou et al., 1990). The β-barrel of p13^{MTCP1} can be classified as an orthogonal barrel ($n < S < 2n$; Murzin et al., 1994a) which falls in one of the categories of barrel structures with good β-sheet geometries in which residues can fill the interior with minimum stress. Regarding its n and S values, it is comparable to the β-barrels found in beef liver catalase (Fita and Rossmann, 1985), streptavidin (Hendrickson et al., 1989) and cyclophillin A (Ke et al., 1991), three functionally unrelated proteins that share this common structural motif. But, as previously quoted, the topology of the strand arrangement in p13^{MTCP1} is markedly different.

The mean slope of the strands to the axis of the barrel found in p13^{MTCP1} is $44 \pm 2°$, and the mean radius of the barrel is 7.4 ± 0.5 Å, in good agreement with the theoretical values calculated from S and n (43° and 7.9 Å, respectively). As usually observed in

Table 2. Experimental constraints and structural parameter statistics of the 20 DYANA conformers representing the solution structure of p13^{MTCP1}

Distance constraints			
	Intraresidue	340	
	Sequential	417	
	Medium-range	88	
	Long-range	408	
	Constraints per residue	18	
Dihedral constraints			
	ϕ	39	
	χ_1	25	
Parameter DYANA			
Target function (Å^2)		2.36 ± 0.32	
Upper-limit violations			
	Number > 0.2 Å	5.0 ± 3.0	
	Sum of violations (Å)	14.8 ± 1.10	
	Maximum violation (Å)	0.34 ± 0.06	
Dihedral angle violations			
	Number $> 5°$	0	
	Sum of violations (°)	9.0 ± 2.50	
	Maximum violation (°)	3.10 ± 1.10	
Van der Waals violations			
	Number > 0.2Å	0	
	Sum of violations (Å)	4.60 ± 0.60	
	Maximum violation (Å)	0.17 ± 0.03	
Rmsd values (Å)			
	Residues 1–107 (all)	BA[a]/HA[b]	$2.45 \pm 0.67/2.74 \pm 0.51$
	Residues 11–103	BA[a]/HA[b]	$1.07 \pm 0.19/1.71 \pm 0.17$
	Residues 11–47 (motif 1)	BA[a]/HA[b]	$0.60 \pm 0.15/1.32 \pm 0.15$
	Residues 67–103 (motif 2)	BA[a]/HA[b]	$0.42 \pm 0.08/1.24 \pm 0.12$

[a] Backbone atoms.
[b] All heavy atoms.

orthogonal barrels, distortion from the ideal geometry flattens the barrel so it has an elliptical cross section rather than a circular one (Figure 7). Strands B and F form the corner strands of the ellipse, whereas it is usually observed that the corners correspond to the β-sheet motif connection strands. Moreover, no disruption is observed in the pattern of hydrogen bonds in these strands, whereas it is generally reported that unusually small numbers of hydrogen bonds are formed by at least one of the corner strands to one of the neighboring strands (Murzin et al., 1994b). Side chains at the interior of the barrel are mostly hydrophobic (Figure 7). Polar or charged residues occur at both ends of the barrel and are oriented so that their polar side chains point to the exterior. Thus, the interior of the barrel is highly non-polar and forms a densely packed hydrophobic core. The tilt of the strands is such that side chains in the interior do not form layers that have any simple relation to the symmetry of the barrel. This irregular arrangement of residues, when combined with the heterogeneous nature of side chains, has been suggested to be responsible for the strong tendency for the cross section of the orthogonal barrel to be distorted toward a more or less elliptical geometry (Chou et al., 1990). This elliptical cross section of the β-barrel has the effect of moving the two sides closer together, and large residues on these sides come into contact. This allows the barrel to exclude bulk solvent from the interior and display favorable intramolecular packing interaction. The distribution of the hydropho-

Table 3. Regular β-sheet hydrogen bonds identified in the 20 DYANA conformers of p13^{MTCP1}

Strand A	Strand B	Strand C	Strand D	Strand H	Strand G	Strand F	Strand E	Strand A
	NH23 - - -	**CO27**						
NH14 - - -	**CO22**							
CO14 - - -	**NH22**							
	NH21 - - -	**CO29**						
	CO21 - - -	**NH29**						
				CO96 - - -	NH93			
				NH96 - - -	CO93			
			NH46 - - -	CO97				
			CO46 - - -	NH97				
		NH30 - - -	**CO45**					
		CO30 - - -	**NH45**					
NH16 - - -	**CO20**							
	CO19 - - -	NH31						
				CO98 - - -	NH91			
				NH98 - - -	**CO91**			
			NH44 - - -	**CO99**				
			CO44 - - -	**NH99**				
				NH100 - - -	**CO89**			
		NH32 - - -	**CO43**					
		CO32 - - -	**NH43**					
			NH42 - - -	**CO101**				
			CO42 - - -	**NH101**				
					NH87 - - -	CO75		
		NH34 - - -	CO41	**CO102 - - -**	**NH86**			
				NH102 - - -	**CO86**			
						CO76 - - -	**NH72**	
					CO85 - - -	**NH77**		
					NH85 - - -	**CO77**		
							NH71 - - -	**CO11**
						CO78 - - -	**NH70**	
						NH78 - - -	**CO70**	
							CO69 - - -	NH13
							NH69 - - -	**CO13**
							CO67 - - -	NH15
					CO83 - - -	**NH79**		
			CO40 - - -	**NE103**				
		NH36 - - -	CO39					

Hydrogen bonds are listed if they are identified in at least 10 of the 20 DYANA conformers. Hydrogen bonds with corresponding slow exchanging amide protons are indicated in bold characters. The criteria used for the identification of a hydrogen bond are that the proton-acceptor distance must be less than 2.4 Å, and the angle between the donor-proton bond and the line connecting the acceptor and donor heavy atoms must be less than 35°.

bic side chains at the interior of the barrel of p13^{MTCP1} is markedly asymmetric. All aromatic side chains are concentrated in one face of the ellipse, roughly delimited by the short strands F, E, A and B. Most of the long-chain aliphatic residues are concentrated on the other face, on the long strands H, G, D and C. This asymmetric distribution probably reduces the destabilizing sterical constraints among the bulky aromatic groups. The fact that numerous aromatic side chains are deeply buried in the hydrophobic interior of the barrel can explain some unusual features observed in the 2D spectra of p13^{MTCP1}. Thus, the strikingly upfield shifted chemical shifts exhibited by the aromatic protons of Trp^{69} (see Table 1) can be easily explained

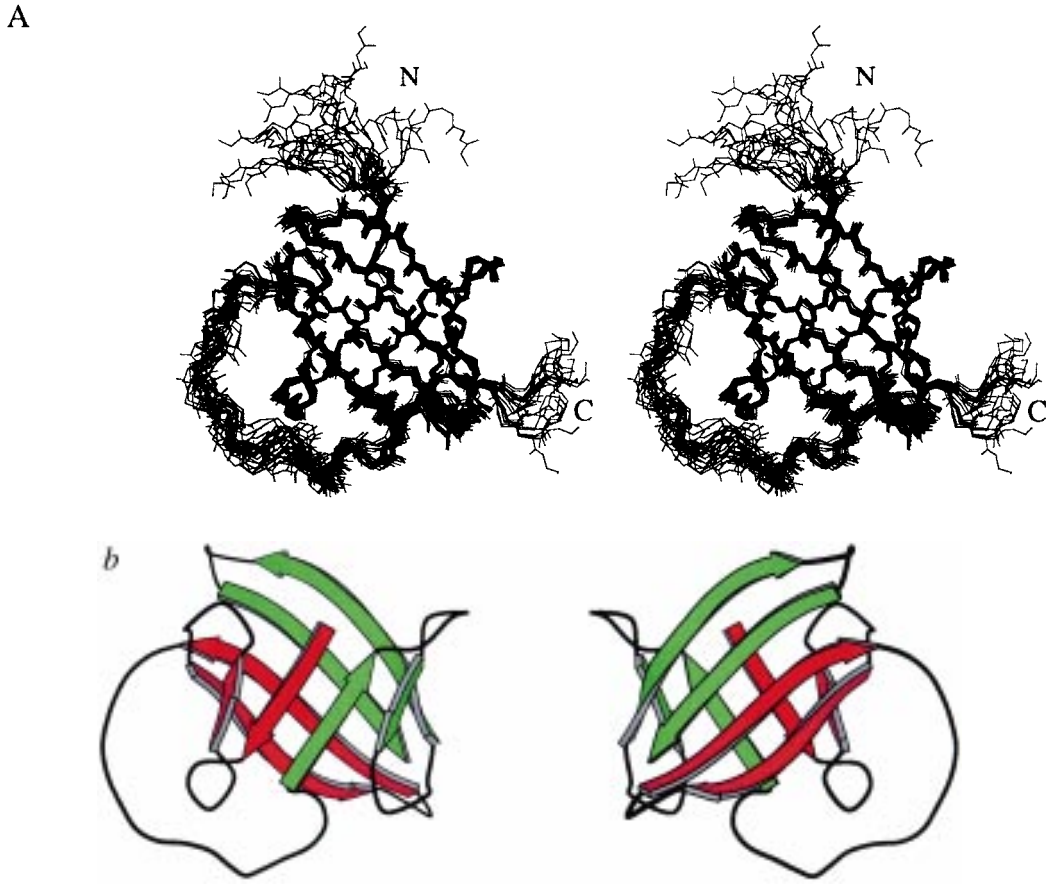

Figure 5. The 3D structure of p13^{MTCP1}. (A) Stereoview of the 20 best structures of p13^{MTCP1}, superimposed over the backbone heavy atoms N, C^{α} and C for residues 11–103. Only backbone atoms are shown. (B) Two views of a ribbon diagram (Kraulis, 1991) of the energy-minimized average structure of p13^{MTCP1}. The two views are related by an $\approx 180°$ rotation about the vertical axis of the barrel. The strands belonging to each of the β-sheet motifs are colored in green and red, respectively.

by ring currents from the surrounding residues Tyr^{21}, Trp^{29}, Tyr^{77} and Trp^{85}. Moreover, the proton resonances of the hydroxyl groups of Tyr^{21} and Tyr^{77}, whose side chains point to the interior of the barrel, are easily identifiable in the 2D NOESY spectra. The outside of the barrel is predominantly polar, although there are a number of non-polar residues.

Oncogenesis arises from various molecular mechanisms which generally block cell apoptosis or deregulate cell division. Oncoproteins participating in this process act at all cellular levels. The fact that p13^{MTCP1} does not belong to any known structural family of oncogenic proteins and that no molecular partners have been identified to date, precludes any conclusion on its mechanism of action based solely on its 3D structure. Nevertheless, when considering the 3D structure of p13^{MTCP1}, its high sequence homology with p14^{TCL1} which is implicated in similar diseases, and general features about macromolecular interactions (Janin and Chothia, 1990; Janin, 1996, 1997), we can propose regions of p13^{MTCP1} that may interact with a molecular partner. Protein–protein, or protein–nucleic acid, recognition results from the assembly of complementary surfaces on two molecules that form a stable, albeit non-covalent, specific complex. The physical chemical basis of the stability (Janin and Chothia, 1990; Janin, 1996, 1997) is reasonably well understood for systems that undergo no large conformation change. The interfaces are large and close-packed, they exclude water, and buried polar groups form hydrogen bonds and salt bridges. It is generally thought, and verified, that the proteins which bind to a same partner share an identical or a very similar binding site and amino acids that are crucial for the interaction are highly conserved. In addition to the binding site itself, amino acids which contribute

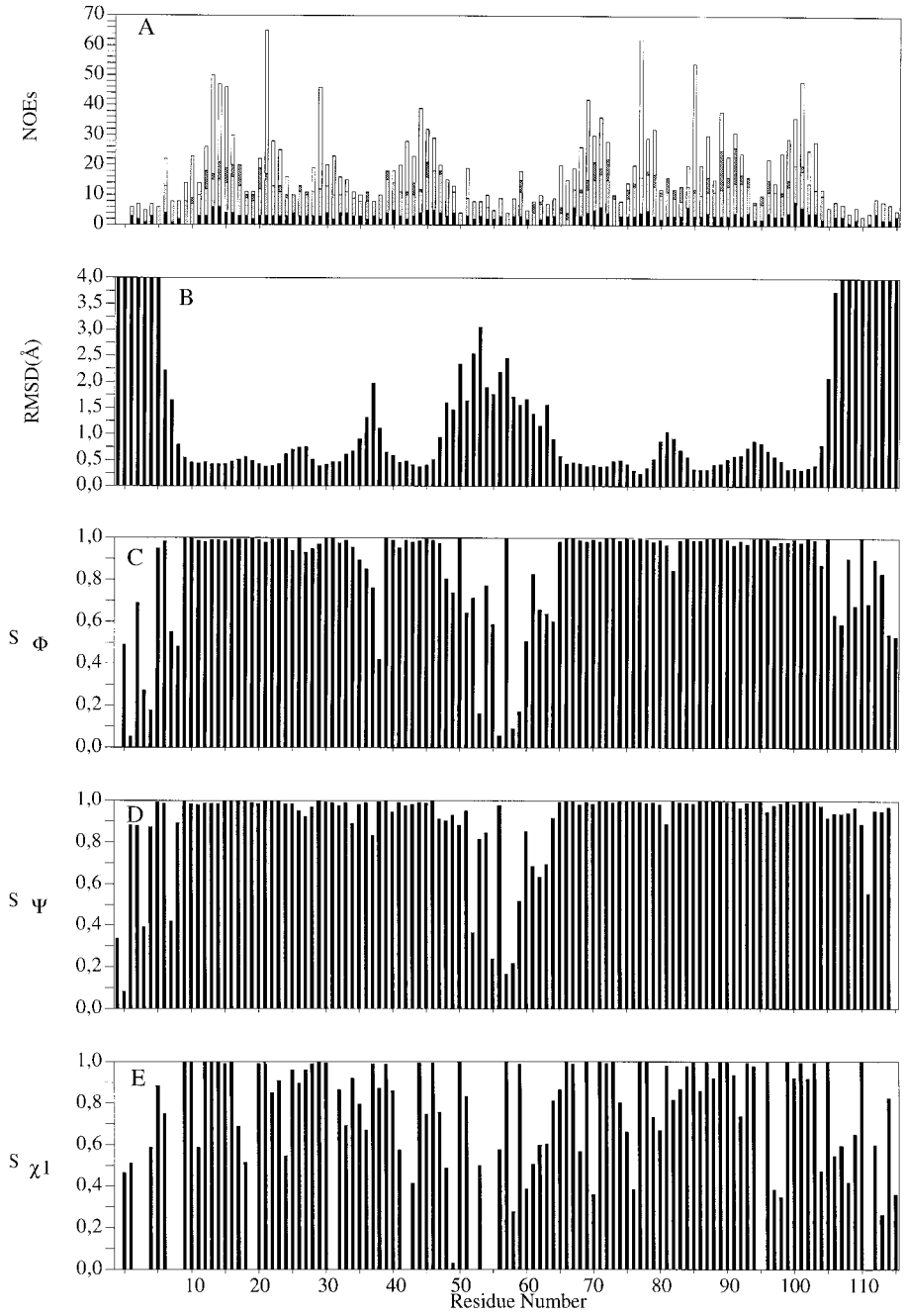

Figure 6. Parameters characterizing the final 20 DYANA structures of p13^{MTCP1}, plotted as a function of residue number. (A) Upper-bound distance restraints used in DYANA. NOE categories are shown as follows: intraresidue, black; sequential, light shaded; medium-range ($2 \leq i - j \leq 4$), dark shaded; long-range ($i - j \geq 5$), open. NOEs are counted twice, once for each proton involved. (B) Rms deviation from the mean structure for the backbone heavy atoms (N, C^{α}, C and O) following superposition over residues 11–103. (C, D, E) Angular order parameters for the backbone ϕ, Ψ and side-chain χ_1 dihedral angles. Gaps in the χ_1 plot are due to glycine and alanine residues.

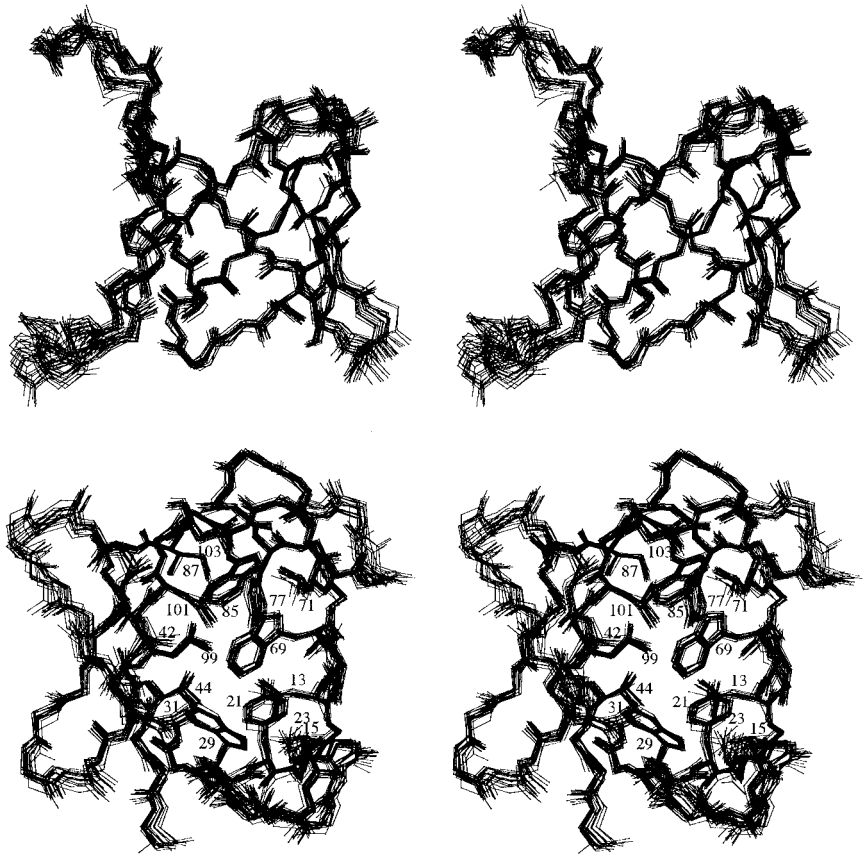

Figure 7. Two stereoviews of the superposition of the β-barrel found in the 20 DYANA conformers of p13^{MTCP1}. In the bottom view, showing the interior of the barrel, the side chains facing the interior of the barrel are reported and labelled.

to the stability of the protein scaffold are also highly conserved. Based on a comparison of the highly homologous sequences (40% identity, 59% homology) of p13^{MTCP1} and p14^{TCL1}, it has been proposed that these two oncogenic proteins share a common structure, and different studies indicate that they may also share a similar mechanism of action (Thick et al., 1996). With 33% identity, the long loop connecting the two β-motifs is the least homologous region between the two proteins. This suggests that this loop could be reasonably discarded as being involved in an interaction common to p13^{MTCP1} and p14^{TCL1}. On the other hand, the amino acids involved in the β-barrel are highly conserved: 75% of the residues are similar, and the homology rises to 80% (50% identity) when considering the residues located on the inside of the barrel, with all differences located on the edges of the two openings of the barrel. We note that, contrary to the eight-stranded up-and-down 'empty barrel' found in the superfamily of proteins that includes, for instance, the lipid-binding proteins (Banaszak et al., 1994) where the barrel acts as a container for chemically quite diverse hydrophobic ligands, there is no example in the literature where the hydrophobic core of 'filled barrels' supports any activity. In these proteins, the binding sites are more likely to occur in loops emerging from the barrel itself (Branden and Tooze, 1991). p13^{MTCP1}, and presumably p14^{TCL1}, falls in the filled barrels class, suggesting that the high conservation of the amino acids involved in the β-barrel is only due to the presence of this common scaffold. Considering the β-pleated loops emerging from the β-barrel, we note that the corresponding 'staves' of the β-barrel form a large concave surface (about 1550 Å^2) which might be considered as a potential interaction surface (Figure 8). Among 22 solvent-exposed residues on this surface in p13^{MTCP1}, 14 are conserved in p14^{TCL1}, including all the hydrophobic residues (45% of the solvent-exposed residues). In p13^{MTCP1}, the other solvent-exposed residues are

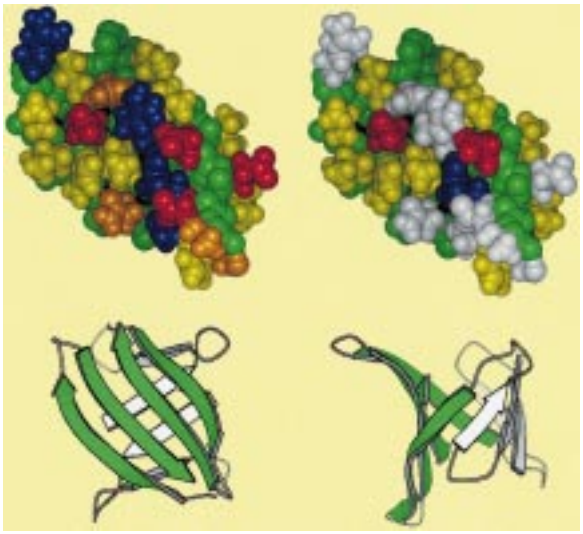

Figure 8. The putative interaction surface of p13^{MTCP1}. (Top) Two ribbon diagrams of the β-barrel showing the β-pleated loops in green. (Bottom) CPK view of the interaction surface. Hydrophobic residues are colored in yellow, polar in orange, negatively charged in red, positively charged in blue, and the backbone atoms in green. In the left view, residues which are not common to p13^{MTCP1} and p14^{TCL1} are reported in white.

equally distributed among polar (Thr^{37}, Ser^{38}, Gln^{45}, Gln^{88}), acidic (Glu^{34}, Glu^{35}, Glu^{36}, Glu^{98}) and basic residues (Arg^{41}, Arg^{43}, Arg^{94}, Lys^{102}). They are less conserved in p14^{TCL1} except for Glu^{98}, which is found in the middle of a highly conserved hydrophobic cluster, and for Glu^{34} and Arg^{41}. These latter two residues are found in a more polar and variable region of the concave surface, since two additional residues and a higher proportion of basic residues are observed in p14^{TCL1} (see Figure 1). Hydrophobic residues are found commonly involved in various intermolecular interactions, including either protein–protein or protein–nucleic acid complexes. Clusters of basic residues are found, for instance, specifically involved with DNA recognition, but the presence of numerous negatively charged residues in the putative interaction surface of p13^{MTCP1} is unlikely to occur in the protein–DNA complex. It rather suggests specific interactions with a protein partner. These assumptions remain very speculative, and we are expecting more direct evidence from biological studies under way in our laboratories.

Conclusions

The solution structure of the human oncogenic p13^{MTCP1} protein has been obtained from homonuclear NMR methods. Both the rmsd and angular order parameters indicate that the structure is resolved with a good accuracy, representing a significant achievement for a non-enriched protein of this size. The 3D structure of p13^{MTCP1} appears to be constituted of an eight-stranded antiparallel β-barrel, a motif known to support a great variety of functions, which presents an original strand arrangement. A comparative analysis of the primary structures of p13^{MTCP1} and p14^{TCL1} combined with the tertiary structure of p13^{MTCP1} allowed us to propose that the two β-pleated loops emerging from the β-barrel might constitute a potential binding site at the surface of the protein. This proposal could be verified by site-directed mutagenesis, for which the knowledge of the 3D structure is an essential tool. Thus, the present work constitutes an important step for the study of biological processes involved in mature T-cell leukemias.

Acknowledgements

We thank Dr. L. Chiche (Centre de Biochimie Structurale (CBS), Montpellier) for helpful discussions. The authors are very grateful to Dr. R. Ghirlando (CBS, Montpellier) for a critical reading of the manuscript. This work was supported by grants from the Ligue Nationale contre le Cancer and from the Association pour la Recherche sur le Cancer.

References

Banaszak, L., Winter, N., Xu, Z., Bernlohr, D.A., Cowan, S. and Jones, T.A. (1994) In *Advances in Protein Chemistry*, Vol. 45 (Ed., Schumaker, V.), Academic Press, San Diego, CA, pp. 89–149.

Barthe, P., Yang, Y.-S., Chiche, L., Hoh, F., Strub, M.-P., Guignard, L., Soulier, J., Stern, M.-H., van Tilbeurgh, H., Lhoste, J.-M. and Roumestand, C. (1997) *J. Mol. Biol.*, **274**, 801–815.

Branden, C.-I. and Tooze, J. (1991) *An Introduction to Protein Structures*, Garland, New York, NY.

Braunschweiler, L. and Ernst, R.R. (1983) *J. Magn. Reson.*, **53**, 521–528.

Chou, K.-C., Heckel, A., Némethy, G., Rumsey, S., Carlacci, L. and Sheraga, H.A. (1990) *Proteins*, **8**, 14–22.

Croce, C.M. (1987) *Cell*, **49**, 155–156.

Dalhuin, C., Wieruszeski, J.M. and Lippens, G. (1996) *J. Magn. Reson.*, **B111**, 168–170.

Dallapiccola, B., Alimena, G., Chessa, L., Gastaldi, R., De Rossi, G., Semenzato, G., Quinti, I. and Pandolfi, F. (1984) *Int. J. Cancer*, **34**, 171–176.

Davey, M.P., Bertness, V., Nakahara, K., Johnson, J.P., McBride, O.W., Waldmann, T. and Kirsch, I.R. (1988) *Proc. Natl. Acad. Sci. USA*, **85**, 9287–9291.
Davis, D.G. and Bax, A. (1985) *J. Am. Chem. Soc.*, **107**, 2820–2821.
Englander, S.W. and Wand, A.J. (1987) *Biochemistry*, **26**, 5958–5962.
Fisch, P., Forster, A., Sherrington, P.D., Dyer, M.J. and Rabbit, T.H. (1993) *Oncogene*, **8**, 3271–3276.
Fita, I. and Rossmann, M.G. (1985) *Proc. Natl. Acad. Sci. USA*, **82**, 1604–1608.
Fu, T.-B., Virgilio, L., Narducci, M.G., Facchiano, A., Russo, G. and Croce, C.M. (1994) *Cancer Res.*, **54**, 6297.
Goyns, M.H., Hammond, D.W., Harrison, C.J., Menasce, L.P., Ross, F.M. and Hancock, B.W. (1993) *Leukemia*, **7**, 848–852.
Güntert, P., Mumenthaler, C. and Wüthrich, K. (1997) *J. Mol. Biol.*, **273**, 283–298.
Haluska, F.G., Tsujimoto, Y. and Croce, C.M. (1987) *Annu Rev. Genet.*, **21**, 321–345.
Hendrickson, W.A., Pahler, A., Smith, J.L., Satow, Y., Merritt, E.A. and Phizakerley, R.P. (1989) *Proc. Natl. Acad. Sci. USA*, **86**, 2190–2194.
Hyberts, S.G., Märki, W. and Wagner, G. (1987) *Eur. J. Biochem.*, **164**, 625–635.
Hyberts, S.G., Goldberg, M.S., Havel, T.F. and Wagner, G. (1992) *Protein Sci.*, **1**, 736–751.
Janin, J. (1996) *Prog. Biophys. Mol. Biol.*, **64**, 145–165.
Janin, J. (1997) *Proteins*, **28**, 153–161.
Janin, J. and Chothia, C. (1990) *J. Biol. Chem.*, **265**, 16027–16030.
Jeener, J., Meier, B.H., Bachman, P. and Ernst, R.R. (1979) *J. Chem. Phys.*, **71**, 4546–4553.
Kadkhodaei, M., Hwang, T.-L., Tang, J. and Shaka, A.J. (1993) *J. Magn. Reson.*, **A105**, 393–399.
Karplus, M. (1963) *J. Am. Chem. Soc.*, **85**, 2870–2871.
Ke, H., Zydowsky, L.D., Liu, J. and Walsh, C.T. (1991) *Proc. Natl. Acad. Sci. USA*, **88**, 9483–9487.
Kraulis, P.J. (1991) *J. Appl. Crystallogr.*, **24**, 946–950.
Kumar, A., Ernst, R.R. and Wüthrich, K. (1980) *Biochem. Biophys. Res. Commun.*, **95**, 1–6.
Laskowski, R.A., MacArthur, M.W., Moss, D.S. and Thornton, J.M. (1993) *J. Appl. Crystallogr.*, **26**, 283–291.
Lippens, G., Dhalluin, C. and Wieruszeski, J.-M. (1995) *J. Biomol. NMR*, **5**, 327–331.
Ludvigsen, S., Andersen, K.V. and Poulsen, F.M. (1991) *J. Mol. Biol.*, **217**, 731–736.
Madani, A., Soulier, J., Schmid, M., Plichtova, R., Lermé, F., Gateau-Roesch, O., Garnier, J.P., Pla, M., Sigaux, F. and Stern, M.-H. (1995) *Oncogene*, **10**, 2259–2262.
Madani, A., Choukroun, V., Soulier, J., Cacheux, V., Claisse, J.F., Valensi, F., Daliphard, S., Cazin, B., Levy, V., Leblond, V., Daniel, M.T., Sigaux, F. and Stern, M.-H. (1996) *Blood*, **87**, 1923–1927.
Marion, D., Ikura, M., Tschudin, R. and Bax, A. (1989) *J. Magn. Reson.*, **85**, 393–399.
Murzin, A.G., Lesk, A.M. and Chothia, C. (1994a) *J. Mol. Biol.*, **236**, 1369–1381.
Murzin, A.G., Lesk, A.M. and Chothia, C. (1994b) *J. Mol. Biol.*, **236**, 1382–1400.
Pardi, A., Billeter, M. and Wüthrich, K. (1984) *J. Mol. Biol.*, **180**, 741–751.
Pearlman, D.A., Case, D.A., Caldwell, J.W., Ross, W.S., Cheatham III, T.E., Fergusson, D.M., Seibel, G.L., Singh, U.C., Weiner, P.K. and Kollman, P.A. (1995) AMBER 4.1, University of California, San Francisco, CA.
Piotto, M., Saudek, V. and Sklenar, V. (1992) *J. Biomol. NMR*, **2**, 661–665.
Pons, J.L., Malliavin, T.E. and Delsuc, M.A. (1996) *J. Biomol. NMR*, **8**, 445–452.
Rabbitts, T.H. (1994) *Nature*, **372**, 143–149.
Rance, M., Sørensen, O.W., Bodenhausen, G., Ernst, R.R. and Wüthrich, K. (1983) *Biochem. Biophys. Res. Commun.*, **117**, 479–495.
Rance, M. (1987) *J. Magn. Reson.*, **74**, 557–564.
Richardson, J.S. (1981) *Adv. Protein Chem.*, **34**, 167–330.
Russo, G., Isobe, M., Gatti, R., Finan, J., Batuman, O., Huebner, K., Nowell, P.C. and Croce, C.M. (1989) *Proc. Natl. Acad. Sci. USA*, **86**, 602–606.
Sherrington, P.D., Fish, P., Taylor, A.M.R. and Rabbitts, T.H. (1994) *Oncogene*, **9**, 2377–2381.
Soulier, J., Madani, A., Cacheux, V., Rosenzwajg, M., Sigaux, F. and Stern, M.-H. (1994) *Oncogene*, **9**, 3565–3570.
Stern, M.-H., Soulier, J., Rosenzwajg, M., Nakahara, K., Canki-Klain, N., Aurias, A., Sigaux, F. and Kirsch, I.R. (1993) *Oncogene*, **8**, 2475–2483.
Taylor, A.M.R., Metcalfe, J.A., Thick, J. and Mak, Y.-F. (1996) *Blood*, **87**, 423–438.
Thick, J., Metcalfe, J.A., Mak, Y.-F., Beatty, D., Minegishi, M., Dyer, M.J.S., Lucas, G. and Taylor, A.M.R. (1996) *Oncogene*, **12**, 379–386.
Virgilio, L., Isobe, M., Narducci, M.G., Carotenuto, P., Camerini, B., Kurosawa, N., Abbas-Ar-Rushdi, Croce, C.M. and Russo, G. (1993) *Proc. Natl. Acad. Sci. USA*, **90**, 9275–9279.
Wishart, D.S., Sykes, B.D. and Richards, F.M. (1991) *J. Mol. Biol.*, **222**, 311–333.
Witzig, T.E., Phyliky, R.L., Li, C.-Y., Homburger, H.A., Dewald, G.W. and Handwerger, B.S. (1986) *Am. J. Hematol.*, **21**, 139–155.
Wüthrich, K., Billeter, M. and Braun, W. (1983) *J. Mol. Biol.*, **169**, 949–961.
Wüthrich, K. (1986) *NMR of Proteins and Nucleic Acids*, Wiley, New York, NY.